Diamond & Related Materials 153 (2025) 112088

Contents lists available at ScienceDirect

Diamond & Related Materials

journal homepage: www.elsevier.com/locate/diamond

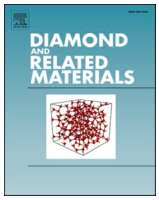

Large diamond disks for ECRH microwave windows in nuclear fusion☆

A. Meier *, G. Aiello, F. Mazzocchi, T. Scherer, S. Schreck, P. Spaeh, D. Strauss

IAM, Karlsruhe Institute of Technology (KIT), 76344 Eggenstein-Leopoldshafen, Germany

ARTICLE INFO

Keywords:
Fusion devices
ECRH system
Diamond window
Dielectric losses
FEM analysis

ABSTRACT

Nuclear fusion devices feature electron cyclotron resonance heating systems for plasma heating and stabilization, with diamond windows acting as vacuum and safety confinement barriers. Diamond is the only option for long-pulse operation in the MW-range applications, given its exceptional combination of optical, thermal and mechanical properties. Dielectric measurements have qualified almost one hundred disks of artificial diamond for their integration into metallic structures to form the complete windows. Optical and mechanical investigations of the disks, together with dedicated numerical analyses of the windows, complete the characterization of these essential components in nuclear fusion.

1. Introduction

In electron cyclotron resonance heating (ECRH) systems for nuclear fusion [1,2], large-area diamond disks are used in transmission windows [3]. The polycrystalline diamond disks produced by microwave plasma assisted chemical vapor deposition (MPA CVD) process have outstanding optical, thermal and mechanical properties allowing transmission of mm-wave beams into the fusion plasma in MW power range and long-pulse operations with minimal losses. No alternative material may be used in this context. Microwave radiation is required in the plasma for heating, non-inductive current drive and control of plasma magneto-hydrodynamic (MHD) instabilities such as the neo-classical tearing modes (NTMs). Diamond has a very high thermal conductivity (5 times higher than copper conductivity), remarkably high thermal shock resistance, low thermal expansion, as well as high strength, stiffness and hardness [4]. The disks are integrated into metallic structures, forming the complete window. Diamond allows a small absorption of the power of the beam which is transmitted, low temperatures and thermal gradients with consequent low stresses generated in the window. These windows serve as vacuum output windows in microwave sources (gyrotrons) and as vacuum and safety barriers (tritium and other hazardous materials) on the torus side of fusion machines, mounted within waveguide. There are different configurations of such diamond windows used in machines like W7-X [5,6], ASDEX Upgrade [7] and future machines like ITER [8] and European DEMO [9].

A typical arrangement of a torus window assembly is shown in Fig. 1. The diamond disk is brazed to copper cuffs, welded then to a metallic housing which protects the disk from any external mechanical loads. The disks have a typical thickness in the range of 1 to 2 mm, depending on the resonance condition with the microwave beam wavelength (to avoid any reflection back to the gyrotrons). The diameter ranges typically from 70 mm up to about 110 mm. Developments are ongoing to enable diamond disks with diameter up to 180 mm, meetings the needs of Brewster-angle broadband window solutions in DEMO [10]. The development of MPA CVD diamond produced by European manufacturers as a window material has been supported for over 20 years by dielectric low power measurements and material characterization at Karlsruhe Institute of Technology (KIT). The loss tangent parameter is fundamental to qualify the disks for their integration into the metallic structures.

In this paper, the experimental setups, the basic evaluation methods and the results of the dielectric measurements are described and discussed. Furthermore, examples of mechanical tests and numerical analyses which have complemented the development of the diamond windows are reported. The output of the dielectric measurements is used as input for the thermal and structural analyses, which are carried out to assess the structural integrity of the window.

2. Dielectric measurements

The dielectric properties of the diamond disks, i.e. the loss tangent ($\tan\delta$) and permittivity (ε_r), have been measured by hemispherical and spherical Fabry-Perot resonators at KIT. Gaussian linearly polarized

☆ This article is part of a special issue entitled: Ndnc2024 published in Diamond & Related Materials

* Corresponding author.
E-mail address: andreas.meier@kit.edu (A. Meier).

https://doi.org/10.1016/j.diamond.2025.112088
Received 17 December 2024; Received in revised form 6 February 2025; Accepted 6 February 2025
Available online 7 February 2025

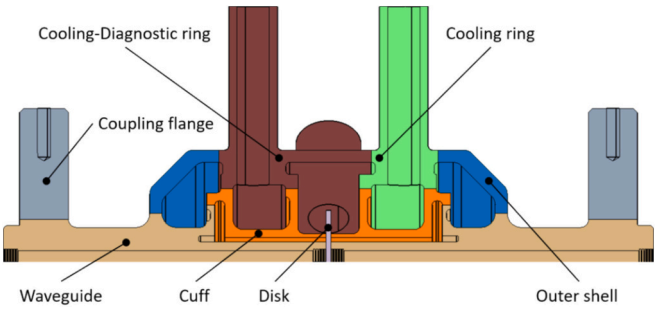

Fig. 1. Example of diamond window designed for the torus side of the ITER ECRH system.

transverse electro-magnetic fundamental modes (TEM00q, q: mode number), which have no components in the direction of propagation, are used for the investigations.

2.1. Hemispherical resonator

In the open hemispherical resonator, the coupled electromagnetic wave is focused by a curved mirror onto a flat mirror. As shown in Fig. 2, the sample material is placed on the plane mirror. The resonant frequency f and its half-bandwidth Δf for the empty and filled (with sample) resonator are measured and compared to determine the tanδ. The basic formula is given by:

$$\tan\delta = F_F\left(\frac{1}{Q_m} - \frac{1}{Q_0} \bullet F_L\right)$$

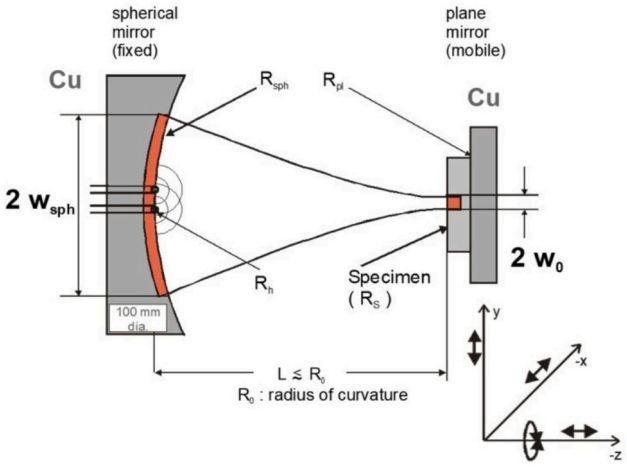

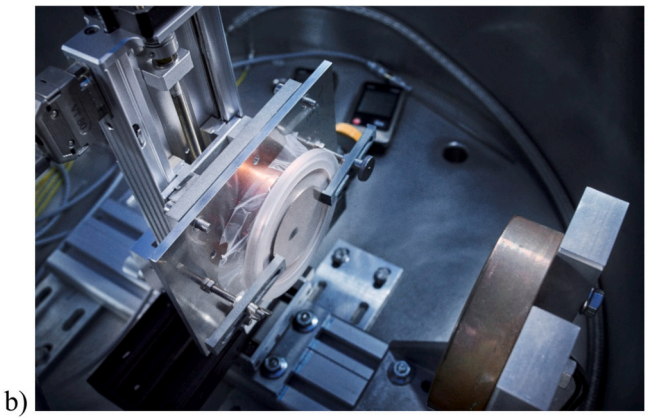

Fig. 2. Schematic arrangement (a) and experimental setup (b) of the hemispherical Fabry–Perot resonator working in the range 130–170 GHz.

where the quality factor Q is the ratio f/Δf for the filled (Q_m) and empty (Q_0) resonators. It represents the ratio of the average energy stored in the resonator to the energy dissipated per oscillation period. The corrective factor F_F describes the effective portion of the sample in the resonator while the loading factor F_L is the quality ratio of the empty resonator and the resonator loaded with a loss-free sample (tanδ = 0).

Fig. 3 shows that the *E*-field strength at the metal mirror surface is always zero while on the other side of the sample, a resonant or anti-resonant condition may occur - depending on the chosen probing frequency. $N_{\lambda/2}$ represents the number of half- wavelengths, and the amplitude of the *E*-field can be set to have surface-sensitive (anti-resonant) or bulk (resonant) measurements of tanδ. This an important feature allowing for the detection of impurities on the surfaces which might lead to high values of tanδ. Furthermore, the set-up allows moving the sample in the vertical plane and therefore it enables homogeneity measurements of the parameter over the sample surface. Statistical values D10 decile, D50 median and D90 decile can be determined from these spatially resolved measurements. The D10, D50 and D90 mean values refer respectively to 10 %, 50 % and 90 % of the inspected area. The permittivity ε_r is determined with a more stable arrangement (fixed sample mirror) in the frequency range 90 to 100 GHz and it can be iteratively calculated using the following transcendental equation:

$$\frac{1}{\sqrt{\varepsilon_r}} tan\left(\frac{2\pi f_m}{c}\sqrt{\varepsilon_r}d - \Phi_t\right) = -tan\left(\frac{2\pi f_m}{c}b - \Phi_b\right)$$

where d is the sample thickness, b is the resonator length reduced by d and Φ_t and Φ_b are phase terms described in [11].

2.2. Spherical resonator

The open spherical setup allows high-resolution point measurements in the range up to about tanδ ~$2{\cdot}10^{-6}$. Two spherical mirrors (curvature radius of 178 mm, silver coated) in an almost concentric geometry are used, which concentrate the electric field at the center of the resonator, as shown in Fig. 4. The resonator length L_{res} is about 335 mm. The Q-factor for the empty resonator with the above structure is between 550 k and 900 k, depending on the exact resonator geometry, the mirror and coupling materials, as well as factors such as frequency / mode number, resonator length and laboratory environment (e.g., humidity). In the loaded case, the sample in the center of the resonator is moved longitudinally through the electromagnetic field in equidistant steps.

The dielectric losses in the area of the beam waist (~20 mm) are determined using the IT method [12]. The reproducibility of the measurements is ensured by comparative measurements on reference samples (Table 1). The arrangement in Fig. 4 also allows measurements of loss tangent on brazed CVD diamond structures. A very important feature as the potential degradation of the tanδ induced by the brazing cycle (e.g., surface contamination by evaporated materials in the vacuum oven) can be estimated.

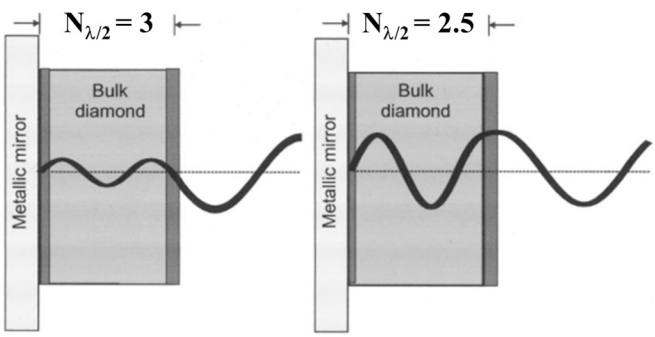

Fig. 3. Resonant (left) / anti-resonant (right) thickness scheme showing minimum / maximum sensitivity to surface losses.

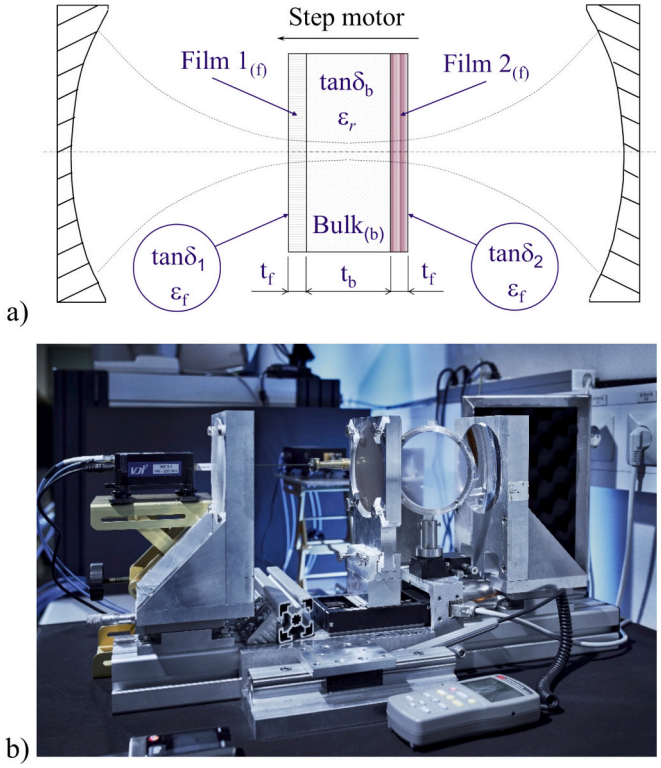

Fig. 4. Schematic arrangement (a) and experimental setup (b) of the spherical Fabry–Perot resonator working in the range 140–220 GHz.

Table 1
Reference disks with dielectric losses.

Reference disk	Resonant frequency GHz	Thickness mm	tanδ 10^{-5}	σ* 10^{-5}
ER_I02	170	1.11	0.6	0.1
70 dB1	170	1.11	1.0	0.1
73 dB1	140	1.81	0.9	0.1

* Standard deviation of all reference measurements.

2.3. Results

The majority of the diamond disks investigated were of optical quality of type IIa or IIb, so that the results essentially reflect the intrinsic level of millimeter wave absorption due to lattice / phonon interaction. Larger extrinsic contributions due to scattering from bulk defects are observed, but they are strongly dependent on growth parameters. The areas of the disks with a greater density of dark microfeatures show higher losses and they are typically located in the outer part of the disks.

These regions may also exhibit birefringence properties due to possible intrinsic radial residual stresses generated by the CVD process. The generation of an ordinary and an extraordinary beam (linearly polarized TEM) lead to a broader resonance curve, as the resonance peaks of both signals could not be clearly separated. This birefringence results in additional intrinsic dielectric bulk losses.

By default, in the measurements, no separation is done between extrinsic and intrinsic contributions. However, in case of high residual stresses in diamond, the loss contribution due to the birefringence is quite significative and it can be clearly seen. No birefringence has been observed in the center of the large-area diamond disks. The dielectric constant was measured at about 95 GHz on about 50 samples and resulted in 5.670 with standard deviation of 0.002.

Point measurements with the spherical resonator in the center of the disk provide an initial indication of the quality of the material, but it does not allow any conclusion about the overall homogeneity of the disk. For this purpose, the mapping process has been established and recognised as a quality assurance process. An example of a typical result of a spatially resolved measurement is the mapping of the diamond disk 73 dB1 (Fig. 5). It has a thickness of 1.8 mm, thus resonant for 140 GHz heating systems, and a diameter of 106 mm. Fig. 6 shows the tanδ distribution over the disk area together with the statistical values. This measurement was carried out at the resonant frequency and it represents therefore the bulk losses in the disk. With reference to Fig. 3, the number of half- wavelengths inside the disk is an integer number ($N_{\lambda/2} = 4$) and no conclusions can be thus drawn about the presence of additional surface losses. The results of the mapping are then parameterized in terms of D50 and D90 mean values and compared to the quantitative acceptance criteria. If lower than the limits, the diamond disks are defined as qualified from the microwave transmission perspective, meaning that they can be integrated in the metallic housing of the windows. The loss tangent measurements represent therefore an important step in the manufacturing of the windows. As an example, the following limits have been defined for the acceptance of the ITER torus ECRH disks: D50 = $3.5{\cdot}10^{-5}$ and D90 = $6.0{\cdot}10^{-5}$.

The variation over approximately 100 diamond disks ranges from $<1{\cdot}10^{-5}$ to $5{\cdot}10^{-5}$ for the D50 quantile and from $1{\cdot}10^{-5}$ to $7{\cdot}10^{-5}$ for the D90 decile. The mean values are given in Table 2. The central measurements however show lower losses and vary between $2{\cdot}10^{-6}$ and $6.5{\cdot}10^{-5}$ over the number of investigated disks.

3. Other characterization activities

3.1. Raman measurements

The density of microfeatures typically correlates with the distance from the disk center. Individual larger features in the disk central region that exhibit conspicuous dielectric losses are investigated using additional methods. Raman analysis is carried out to distinguish diamond phase (sp^3) from non-diamond phase which might occur in these dark structures. A Raman spectrometer with excitation waves in the near ultraviolet, visible and near infrared range is used for these further

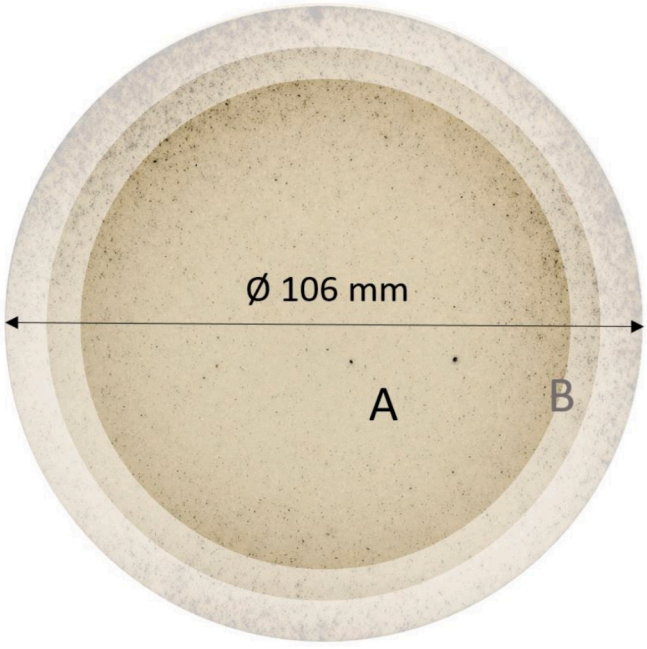

Fig. 5. Diamond disk 73 dB1 with standard (inner region A, Ø 80 mm) and maximum (middle region B, Ø 90 mm) mapping areas.

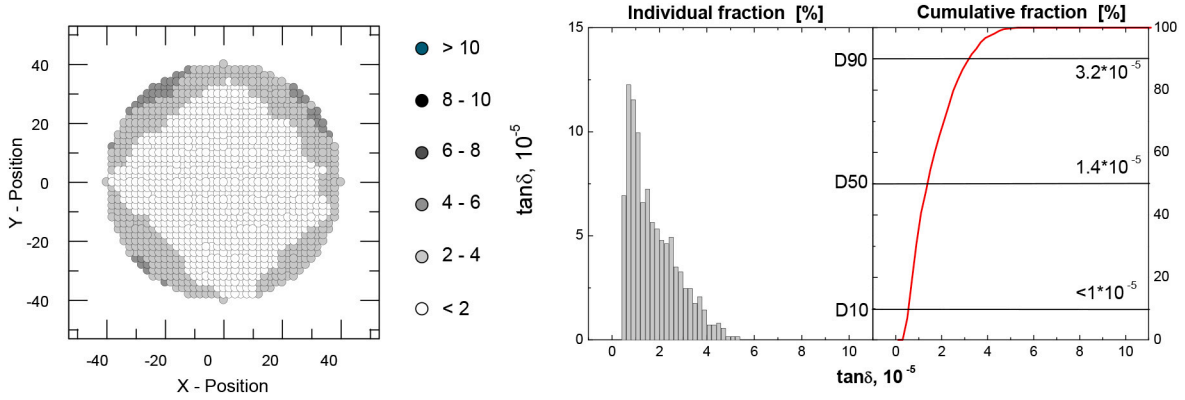

Fig. 6. Typical mapping results with reference to the diamond disk 73 dB1, at the resonant frequency (140 GHz – $N_{\lambda/2} = 4$, bulk losses according to Fig. 3). Point-by-point representation of the individual measurements is shown on the left and the statistical distribution of the individual values on the right.

Table 2
Results of the dielectric measurements of diamond disks in the last two decades for different fusion projects.

Type of windows	Diameter	Measurement diameter standard / maximum	Measurement points @* Typ. / Max.	Relevant number of points @* (standard) D10 / D50 / D90	Dielectric losses tanδ *10^{-5} (mean) D10 / D50 / D90
Gyrotron / Torus	106 mm	80 mm / 90 mm	1257 /1605	126 / 629 / 1131	1.7 / 2.3 / 3.5
Torus (ITER)	70 mm	50 mm / 54 mm	497 / 593	50 / 249 / 447	<1 / 1.7 / 3.5

* Standard step size is 2 mm, spot diameter is approximately 15 mm.

investigations. An optically significant dark microfeature found in the central region of interest in the disk 73 dB1 was compared with a graphitic (sp^2) deposition. Fig. 7 shows the locations of both the microfeature and the intentionally deposited graphitic spot. Thus, the loss tangent measurement over the disk area was repeated, but in anti-resonant case to perform a surface-sensitive measurement of the diamond disk (Fig. 8). A frequency of 158 GHz was selected, turning in a half-integer of the number of half- wavelengths inside the disk ($N_{\lambda/2} \approx$ 4.5). In comparison to Fig. 6, it might be concluded that Fig. 8 shows a clear increase of the dielectric losses only in the area where graphite was deposited and this illustrates the high sensitivity of the resonator setup to sp^2 hybridized components. No other significant increase of the losses could be observed on the disk mapping of Fig. 8, leading to the conclusion that no additional losses occur due to impurities on the disk surface (beyond the graphitic deposition). Finally, Fig. 9 reports the Raman spectra measured in the two locations of Fig. 7.

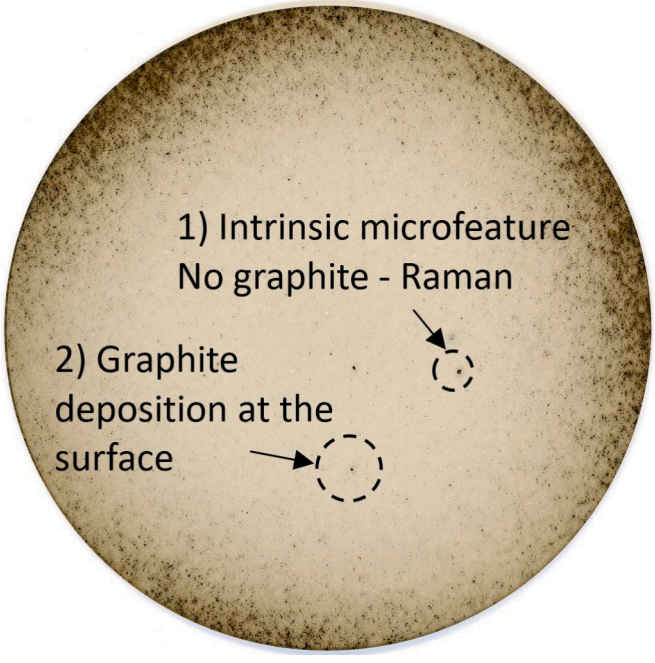

Fig. 7. View of the diamond disk 73 dB1 with 2 points of interest: 1) about 1 mm microfeature and 2) graphitic deposition on the surface with similar size as in 1).

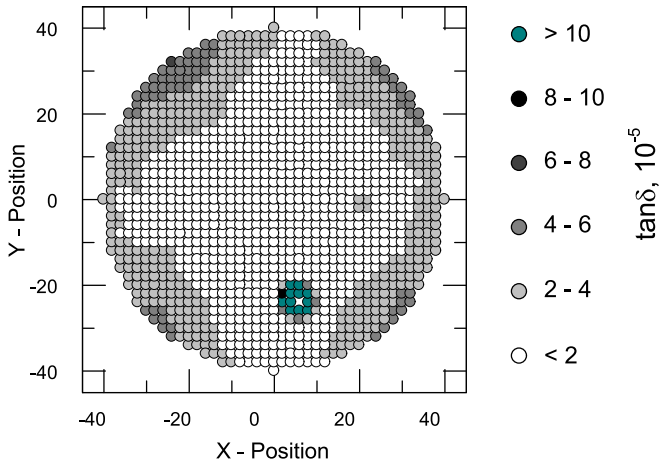

Fig. 8. Mapping result illustrating the strong influence of a graphitic layer/deposition on the measurement. This measurement was performed at surface sensitive frequency and on the right-bottom part, the high value of loss tangent is due to the intentionally graphitic deposition (158 GHz – $N_{\lambda/2} \approx 4.5$, bulk and surface losses according to Fig. 3).

3.2. Microscopy investigations

The diamond disks that are polished after their growth in the microwave reactors are optically transparent. These disks are investigated

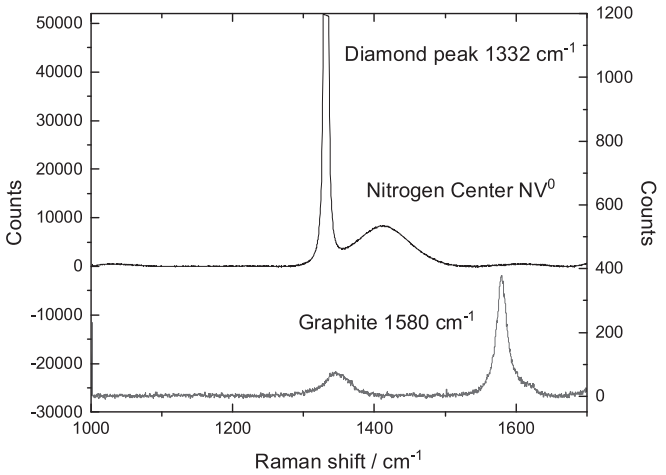

Fig. 9. Raman spectra obtained by 532 nm excitation wavelength in the locations of dark microfeature (upper curve, relates to position no. 1 in Fig. 7) and graphitic deposition area (lower curve, relates to position no. 2).

by a high-resolution digital 3D light microscope to characterize the dark microfeatures, generated during the CVD process, in terms of size and position. These features are considered microcracks where light gets trapped in and therefore appear with a dark color. However, some of them might be decorated by graphite, so microscopy activity is often accompanied by Raman measurements. As already mentioned in §2.3, the high presence of dark microfeatures located in the outer region of the diamond disks contribute to the high losses mainly due to the scattering. In the case of isolated dark microfeatures in the central area of the disks, generally no direct impact has been observed in the loss tangent mapping of the disks.

The microscope allows generating EFI (extended focal imaging) images where the scans at different vertical positions of the disk are combined to one image. The aim in this case, is to determine the size of the feature on the horizontal plane. For instance, Fig. 10a shows a size of about 1 mm for the dark microfeature marked in Fig. 7. Instead, a detailed multilayer scan provides information on the vertical position and configuration of the microfeatures. In the case of the microfeature shown in Fig. 10a, it was observed that the feature is located at about 350 μm from the growth side of the disk and has a vertical size of about 400 μm. It shall be kept in mind that the vertical evolution of the microfeatures is quite complex and the size refers to the upper and lower boundaries of the feature. Furthermore, microscopic images under polarized light did not show any significant increased birefringence behavior (same color pattern) in the area close to the large microfeature with respect to the one characterized by smaller features (Fig. 10b).

3.3. Strength measurements

The ultimate bending strength of diamond is required in the window analyses for the structural integrity check of the disks. This parameter is most determined using three-point bending tests with beam-shaped samples. A uniaxial stress state is present here. However, for diamond used in shape of disks in nuclear fusion, other test methods shall be used considering a thin, disk-shaped geometry. This is the case of methods like ball on ring and ring on ring. In literature, only a few systematic investigations are available [13].

The bending strength was therefore measured on large-area polycrystalline CVD diamond disks (diameter 30 mm, thickness 1.11 mm) of same quality of the ITER torus disks [14]. The bending strength was determined using the double ring method according to DIN 51105. For conservative reasons, the growth side was displaced under tensile stress due to its lower strength values compared to the nucleation side. The average double-ring bending strength of the CVD diamond disks resulted

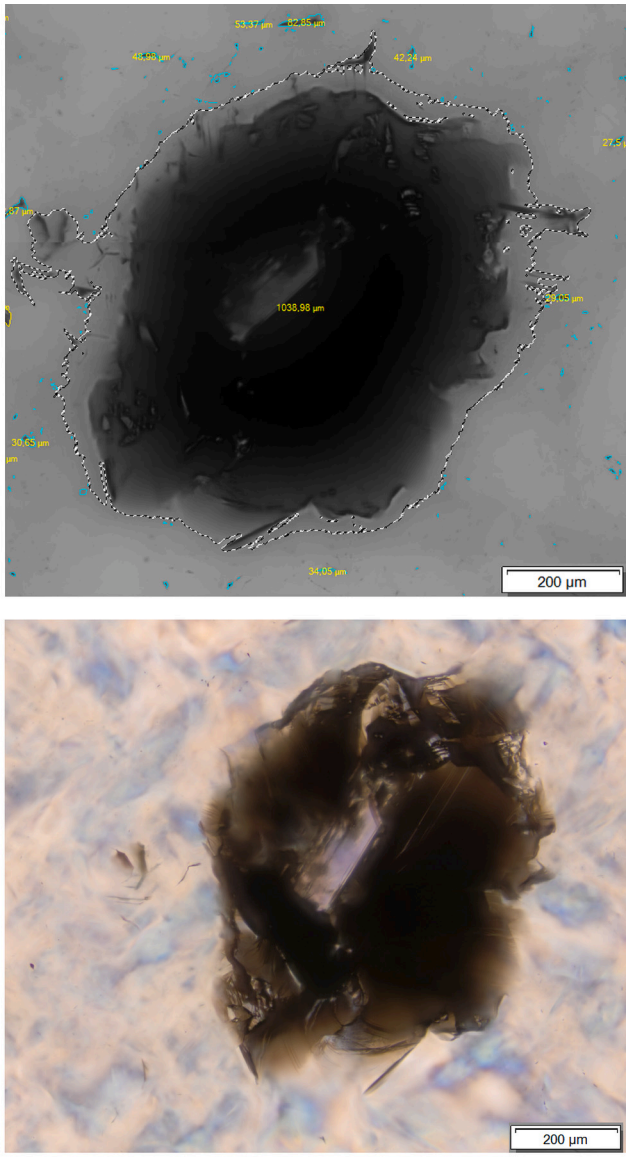

Fig. 10. EFI image of the microfeature marked in Fig. 7 (a) and related polarized light EFI image (b).

314 MPa with a standard deviation of ±17 MPa.

From literature, it turns out that the thermal quality diamond, characterized by a higher density of microfeatures with respect to the optical quality, shows greater values of ultimate strength than the optical one (factor about 1.5 [13]). This might be explained with a kind of toughnening mechanism associated to the large presence of microfeatures. On the other side, one shall look at the main failure mode of the diamond disks, which is represented by the failure to fracture, i.e. the failure due to crack propagation. In that case, fracture toughness shall be considered as main mechanical property, which describes the resistance to crack extension of a material. Measurements of such a parameter for optical and thermal quality diamond are planned with the focus on understanding the role of the microfeatures on the failure due to crack propagation [15]. This kind of investigation is of fundamental importance, considering the safety role of the diamond disks on the torus side of the fusion devices.

4. Numerical analyses

The design of the diamond window is verified by numerical analyses

aiming to check whether temperatures and stresses generated by normal operation and off-normal events are lower than the limits. In this context, the tanδ measurement of the diamond disks provide an important input to the analyses as it allows calculating the power absorbed in the disk during the mm-wave beam transmission. In general, the numerical analyses allow investigating several window designs by calculating temperatures and stresses, so then the design variant leading to the highest safety margins is selected.

Considering the example of the ITER EC torus window, Fig. 11 shows the geometry of the current design used in the analysis. First, steady-state computational fluid dynamics (CFD) conjugated heat transfer analyses were carried out to investigate the cooling and the thermal performance of the window. Temperature-dependent properties for pure copper, CVD diamond and CuCrZr alloy were used. A mass flow rate of 0.087 kg s^{-1} was assumed for the inlet while a reference pressure of 0 Pa was applied to the outlet. The inlet temperature of the water was set to 30 °C. The design beam power of 1.31 MW at the window location was considered to calculate the power absorbed in the disk according to [16]:

$$P_{abs} \simeq \frac{P_{beam}\,\pi\, f\, t\, tan\delta\,(1+\varepsilon_r)}{c_0}$$

where P_{abs} is the absorbed power, $P_{beam} = 1.31$ MW is the beam power, f = 170 GHz is the beam frequency, $t = 1.11$ mm is the disk thickness, $\tan\delta = 2.0{\cdot}10^{-5}$ is the loss tangent, $\varepsilon_r = 5.67$ is the dielectric constant of diamond and c_0 is the speed of light in vacuum. These values translate to an absorbed power of 346 W. The heat generation load was applied to the disk by the zero-order Bessel function which describes the power pattern of the HE_{11} mode beam inside the waveguide lines:

$$q'''(r) = A[J_0(x)]^2, x = 2.405\frac{r}{a}$$

where q''' is the volumetric power density in W m^{-3}, $A = 5.88{\cdot}10^8$ is the normalizing constant, r is the radial coordinate and a = 25 mm is the waveguide aperture. The power density distribution q''' was normalized to obtain the calculated value of absorbed power in the disk. Then, the heat flux of 3882 W m^{-2} was applied to the inner surface of the cuff, as directly exposed to the travelling beam.

Fig. 12 shows the results in terms of temperature profiles along the disk diameter in the symmetry plane of the window. The analysis was run for different values of tanδ, to check the sensitivity of the window

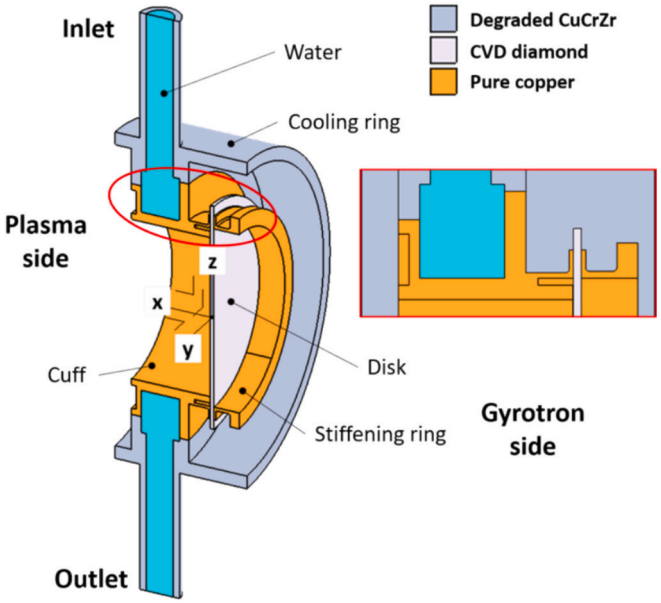

Fig. 11. Window geometry in the CFD conjugated heat transfer analysis.

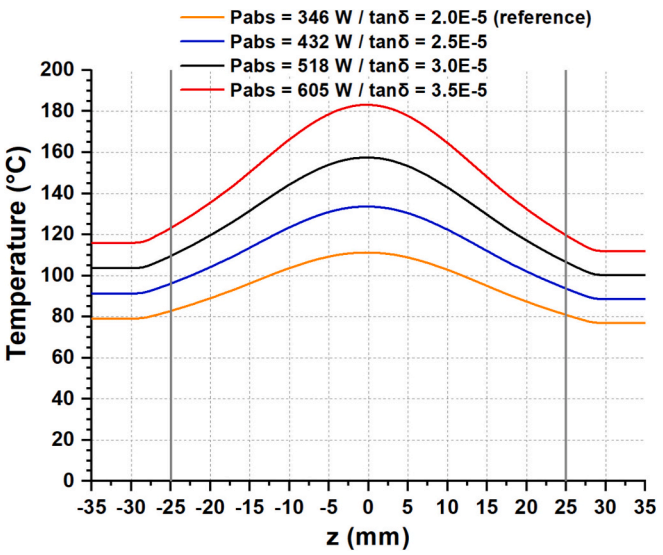

Fig. 12. Sensitivity analysis of the current ITER EC torus window design for the loss tangent parameter. Temperature profiles are shown along the disk diameter in the symmetry plane. Vertical lines show the window aperture.

design against a potential degradation of such an important parameter, which rules the power absorption in the disk. The range was extended from $2.0{\cdot}10^{-5}$ up to $3.5{\cdot}10^{-5}$, the latter corresponding to the acceptance criterion defined for D50 of the tanδ distribution at 170 GHz in the bare ITER disks. With reference to the average D50 = $1.7{\cdot}10^{-5}$ reported in Table 2 for the ITER torus disks, the choice in the analysis of $\tan\delta = 2.0{\cdot}10^{-5}$ as reference case can be considered conservative for taking into account any potential degradation due to brazing and manufacturing. The sensitivity analysis showed that, even in the unlike event of a degradation of the bare disk tanδ, the calculated maximum temperatures are still far from the temperature limit of 250 °C, assumed for diamond. Therefore, the window design can be considered quite robust under the thermal perspective.

A structural analysis was then performed to check, in the reference case, the stresses generated in the window during the worst load case of the disk, i.e. normal operation (NO) plus 2 bar overpressure event. The temperature distribution from the analysis above was applied as load together with the coolant pressure (8.5 bar at the cooling interface). A pressure of 2 bar was additionally applied to the disk and cuff surfaces on the plasma side of the window (Fig. 11). A plastic steady-state structural analysis was carried out. Fig. 13 shows the resulting stress

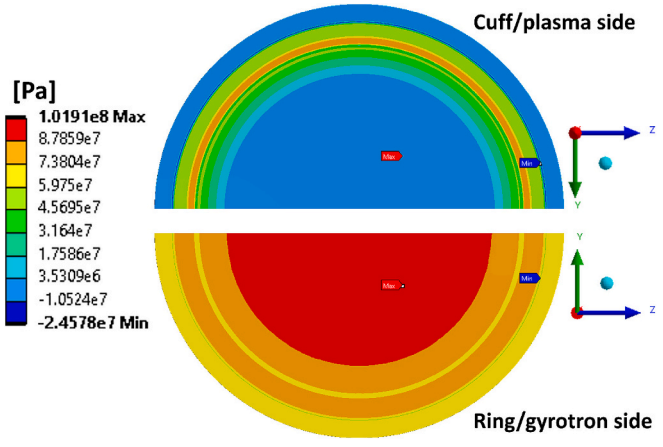

Fig. 13. First principal stress distribution on the two sides of the diamond disk for 2 bar overpressure occurring during normal operation [15].

in the disk. The maximum principal stress is in the range 88–102 MPa in the central area of the disk, on the tensile side. The stress is ~57–88 MPa at the interface region with the ring while 50–63 MPa at the one with the cuff. These stresses in diamond can be safely accepted, when compared to the allowable stress of 150 MPa assumed for diamond. The ultimate bending strength of 1.11 mm optical quality CVD diamond samples (same diamond used in the window) was measured and resulted in the value of 314 MPa [14].

5. Conclusions

The extremely high thermal conductivity and low dielectric losses make CVD diamond suitable for use in highly stressed components in microwave heating systems for nuclear fusion. Consistent further development starting in the 1990s made it possible to produce large-format polycrystalline diamond disks using CVD processes. Characterization in open resonators allowed to determine the dielectric properties, loss tangent and permittivity of well over 100 diamond disks. The investigations were supplemented by microscopic and spectroscopic methods (Raman). The results are the basis for the ongoing quality assurance process and also represent input parameters for the numerical analyses of the windows.

CRediT authorship contribution statement

A. Meier: Writing – original draft, Validation, Methodology, Investigation, Funding acquisition, Formal analysis, Data curation, Conceptualization. **G. Aiello:** Writing – original draft, Visualization, Software, Formal analysis, Conceptualization. **F. Mazzocchi:** Writing – review & editing. **T. Scherer:** Writing – review & editing, Supervision, Project administration, Funding acquisition. **S. Schreck:** Writing – review & editing, Project administration, Data curation. **P. Spaeh:** Writing – review & editing. **D. Strauss:** Writing – review & editing, Supervision, Project administration, Funding acquisition.

Declaration of competing interest

The authors declare the following financial interests/personal relationships which may be considered as potential competing interests: Andreas Meier reports financial support was provided by Eurofusion Consortium. Andreas Meier reports financial support was provided by Fusion for Energy. If there are other authors, they declare that they have no known competing financial interests or personal relationships that could have appeared to influence the work reported in this paper.

Acknowledgments

This work has been supported by Fusion for Energy under the contract No. F4E-OFC-842-SC03. The views and opinions expressed herein reflect only the author's views. Fusion for Energy and ITER Organization are not liable for any use that may be made of the information contained therein. This work has been carried out also within the framework of the EUROfusion Consortium, funded by the European Union via the Euratom Research and Training Programme (Grant Agreement No 101052200 — EUROfusion). Views and opinions expressed are however those of the authors only and do not necessarily reflect those of the European Union or the European Commission. Neither the European Union nor the European Commission can be held responsible for them.

Data availability

The data that has been used is confidential.

References

[1] T. Omori, F. Albajar, T. Bonicelli, G. Carannante, M. Cavinato, F. Cismondi, C. Darbos, G. Denisov, D. Farina, M. Gagliardi, F. Gandini, T. Gassmann, T. Goodman, G. Hanson, M.A. Henderson, K. Kajiwara, K. McElhaney, R. Nousiainen, Y. Oda, A. Oustinov, D. Parmar, V.L. Popov, D. Purohit, S. Laxmikanth Rao, D. Rasmussen, V. Rathod, D.M.S. Ronden, G. Saibene, K. Sakamoto, F. Sartori, T. Scherer, N. Pal Singh, D. Strauß, K. Takahashi, Progress in the ITER electron cyclotron heating and current drive system design, Fusion Engineering and Design 96–97 (2015) 547–552.

[2] T. Franke, G. Aiello, K. Avramidis, C. Bachmann, B. Baiocchi, C. Baylard, A. Bruschi, D. Chauvin, A. Cufar, R. Chavan, C. Gliss, F. Fanale, L. Figini, G. Gantenbein, S. Garavaglia, G. Granucci, J. Jelonnek, G. Suárez López, A. Moro, M. Moscheni, N. Rispoli, M. Siccinio, P. Spaeh, D. Strauss, F. Subba, I. Tigelis, M. Q. Tran, C. Tsironis, C. Wu, H., Zohm, integration concept of an electron cyclotron system in DEMO, Fusion Engineering and Design 168 (2021) 112653.

[3] M. Thumm, State-of-the-art of high power gyro-devices and free electron masers, J. Infrared Millim. Terahertz Waves 41 (2020) 1–140.

[4] D.C. Harris, Infrared Window and Dome Materials, SPIE, Washington, 1992.

[5] R.C. Wolf, S. Bozhenkov, A. Dinklage, G. Fuchert, Y.O. Kazakov, H.P. Laqua, S. Marsen, N.B. Marushchenko, T. Stange, M. Zanini, I. Abramovic, A. Alonso, J. Baldzuhn, M. Beurskens, C.D. Beidler, H. Braune, K.J. Brunner, N. Chaudhary, H. Damm, P. Drewelow, G. Gantenbein, Y. Gao, J. Geiger, M. Hirsch, U. Höfel, M. Jakubowski, J. Jelonnek, T. Jensen, W. Kasparek, J. Knauer, S.B. Korsholm, A. Langenberg, C. Lechte, F. Leipold, H. Trimino Mora, U. Neuner, S.K. Nielsen, D. Moseev, H. Oosterbeek, N. Pablant, E. Pasch, B. Plaum, T. Sunn Pedersen, A. Puig Sitjes, K. Rahbarnia, J. Rasmussen, M. Salewski, J. Schilling, E. Scott, M. Stejner, H. Thomsen, M. Thumm, Y. Turkin, F., Wilde and the Wendelstein 7-X team, electron-cyclotron-resonance heating in Wendelstein 7-X: a versatile heating and current-drive method and a tool for in-depth physics studies, Plasma Phys. Control. Fusion 61 (2019) 014037.

[6] R. Heidinger, G. Dammertz, A. Meier, M. Thumm, CVD diamond windows studied with low- and high- power millimeter waves, IEEE Transaction on Plasma 30 (3) (2002) 800–807.

[7] D. Wagner, J. Stober, F. Leuterer, M. Monaco, S. Müller, M. Münich, C.J. Rapson, M. Reich, M. Schubert, H. Schütz, W. Treutterer, H. Zohm, M. Thumm, T. Scherer, A. Meier, G. Gantenbein, J. Jelonnek, W. Kasparek, C. Lechte, B. Plaum, T. Goodman, A.G. Litvak, G.G. Denisov, A. Chirkov, V. Zapevalov, V. Malygin, L. G. Popov, V.O. Nichiporenko, V.E. Myasnikov, E.M. Tai, E.A. Solyanova, S. A. Malygin, ASDEX Upgrade Team, Status, Operation, and Extension of the ECRH System at ASDEX Upgrade, J. Infrared Milli Terahz Waves 37 (2016) 45–54.

[8] G. Aiello, N. Casal, M. Gagliardi, T. Goodman, M. Henderson, A. Meier, G. Saibene, T. Scherer, S. Schreck, D. Strauss, Design evolution of the diamond window unit for the ITER EC H&CD upper launcher, Fusion Eng. Des. 146 (2019) 392–397.

[9] A. Bruschi, J.P. Hogge, J. Jelonnek, D. Strauss, Ch. Wu, G. Aiello, K. Avramidis, B. Baiocchi, D. Birlan, R. Chavan, I. Chelis, A. Clement, A. Collaku, F. Crisinel, R. Difonzo, B. Ell, F. Fanale, P. Fanelli, L. Figini, E. Gajetti, G. Gantenbein, S. Garavaglia, T.P. Goodman, S. Illy, Z. Ioannidis, J. Jin, G. Latsas, C.L. Marraco Borderas, S. Marsen, A. Moro, M. Noël, D. Peponis, T. Pinna, P. Platania, N. Rispoli, T. Ruess, T. Rzesnicki, A. Salvitti, L. Savoldi, T. Scherer, S. Schreck, A. Simonetto, P. Spaeh, S. Stanculovic, T. Stange, M. Thumm, I. Tigelis, C. Tsironis, D. Wagner, A. Xydou, Conceptual design of a modular EC heating system for EU-DEMO, Nucl. Fusion 64 (2024) 106003.

[10] G. Aiello, K. Avramidis, T. Franke, G. Gantenbein, J. Jelonnek, A. Meier, T. Scherer, S. Schreck, D. Strauss, M. Thumm, M.Q. Tran, C. Wild, E. Woerner, Large area diamond disk growth experiments and thermomechanical investigations for the broadband Brewster window in DEMO, IEEE Trans. Electron Devices 68 (9) (2021) 4669–4674.

[11] P.K. Yu, A.L. Cullen, Measurement of permittivity by means of an open resonator, Proceedings of the Royal Society of London. Series A, Mathematical and Physical Sciences 380 (1778) (1982) 49–71.

[12] I. Danilov, R. Heidinger, New approach for open resonator analysis for dielectric measurements at mm-wavelengths, J. Eur. Ceram. Soc. 23 (14) (2003), 2623–2326.

[13] R. Spörl, The influence of the microstructure on the mechanical strength and the dielectric properties of CVD diamond, KIT PhD Thesis, 2001.

[14] S. Schreck, G. Aiello, S. Dieterle, M. Gagliardi, A. Meier, G. Saïbene, T. Scherer, D. Strauss, ITER ECRH upper launcher diamond window – qualification and testing of a protection important component, Fusion Engineering and Design 136 (Part A) (2018) 472–476.

[15] G. Aiello, P. Estebanez, B. Gorr, A. Meier, S. Schreck, T. Scherer, D. Strauss, C. Wild, E. Woerner, Towards fracture toughness measurements of MPA CVD diamond in nuclear fusion devices, in: Proceedings of the 48th International Conference on Infrared, Millimeter and Terahertz Waves, 17–22 September 2023, Montreal, Canada, IEEE, 2023.

[16] X. Yang, G. Dammertz, R. Heidinger, K. Koppenburg, F. Leuterer, A. Meier, B. Piosczyk, D. Wagner, M. Thumm, Design of an ultra-broadband single-disk output window for a frequency step-tunable 1 MW gyrotron, Fusion Engineering and Design 74 (2005) 489–493.